

Chimeras in Leaky Integrate-and-Fire Neural Networks: Effects of Reflecting Connectivities

N. D. Tsigkri-DeSmedt

*Institute of Nanoscience and Nanotechnology, National Center for Scientific Research “Demokritos”, 15310 Athens, Greece and
Department of Physics, University of Athens, Athens, Greece*

J. Hizanidis

*Institute of Nanoscience and Nanotechnology, National Center for Scientific Research “Demokritos”, 15310 Athens, Greece and
Crete Center for Quantum Complexity and Nanotechnology,
Department of Physics, University of Crete, 71003 Heraklion, Greece*

E. Schöll

Institut für Theoretische Physik, Technische Universität Berlin, Hardenbergstraße 36, 10623 Berlin, Germany

P. Hövel

*Institut für Theoretische Physik, Technische Universität Berlin,
Hardenbergstraße 36, 10623 Berlin, Germany and
Bernstein Center for Computational Neuroscience Berlin,
Humboldt-Universität zu Berlin, Philippstraße 13, 10115 Berlin, Germany*

A. Provata

*Institute of Nanoscience and Nanotechnology, National Center for Scientific Research “Demokritos”, 15310 Athens, Greece
(Dated: Received: March 9, 2022/ Revised version: date)*

The effects of nonlocal and reflecting connectivity are investigated in coupled Leaky Integrate-and-Fire (LIF) elements, which assimilate the exchange of electrical signals between neurons. Earlier investigations have demonstrated that non-local and hierarchical network connectivity often induces complex synchronization patterns and chimera states in systems of coupled oscillators. In the LIF system we show that if the elements are non-locally linked with positive diffusive coupling in a ring architecture the system splits into a number of alternating domains. Half of these domains contain elements, whose potential stays near the threshold, while they are interrupted by active domains, where the elements perform regular LIF oscillations. The active domains move around the ring with constant velocity, depending on the system parameters. The idea of introducing reflecting non-local coupling in LIF networks originates from signal exchange between neurons residing in the two hemispheres in the brain. We show evidence that this connectivity induces novel complex spatial and temporal structures: for relatively extensive ranges of parameter values the system splits in two coexisting domains, one domain where all elements stay near-threshold and one where incoherent states develop with multileveled mean phase velocity distribution.

I. INTRODUCTION

Chimera states, which are characterized by spatial coexistence of coherent and incoherent oscillators, were first introduced in 2002 by Kuramoto and Battogtokh [1] and by Abrams and Strogatz in 2004 [2]. These states appear in systems of nonlocally coupled oscillators as well as in oscillator networks with complex connectivity. In chimera states the coherent parts are characterized by constant mean phase velocity, while the incoherent ones demonstrate an arc-shaped profile of the mean phase velocities [3, 4]. A wide range of neuronal models have been shown to exhibit chimera states, [5–12] The aim of the current study is to investigate the influence of neuron connectivity patterns on the formation of chimera states. For this reason, we consider two kinds of connectivity, nonlocal and reflecting, in the Leaky Integrate-and-Fire (LIF) model, which is one of the classical models in neuroscience [13].

The problem of connectivity in networks composed of neuronal oscillators is of fundamental interest in neuroscience. The human brain consists of approximately 10^{10} nerve cells (neurons) and each of them is linked with up to 10^4 other neurons via synapses. Even with today’s most advanced Magnetic Resonance Imaging (MRI) and functional Magnetic Resonance Imaging (fMRI) equipment detailed connectivity patterns are not exactly known and they are the subject of intense international research, both experimentally and computationally [14, 15]. It is widely believed that high connectivity is relevant in cognition, intelligence and creativity, while low or interrupted connectivity is related to mental disorders, such as schizophrenia, Alzheimer or Parkinson [16].

Despite the difficulties in mapping neuron connectivity patterns, MRI and fMRI studies have revealed local spatial structures connecting the loci in the human brain [17, 18]. In particular, in ref. [18] Finn et al. propose that it is even possible to identify a person from the “fingerprints” of their brain connectivity patterns, as mapped

by fMRI. The experimental output of these studies is often used as input in numerical experiments aiming to understand the flow of information in the brain. Information is exchanged between neurons as electrical signals which trigger synchronous, delayed or asynchronous responses propagating the information. During these exchanges collective neuron response can be understood as a pattern.

One might hypothesize that each synchronization pattern describes a “memory” (or any cognitive activity) and can be recalled and reproduced later if the same or similar electrical signals arrive. Once the connectivity is established and remains unchanged in time the same input stimulus will create the same synchronization effect in the neurons involved and this effect corresponds to recalling a “memory” pattern. This view explains why “memories” fade away with time: once enough of the synapses break or neurons die (due to aging, or disease, or accident) then it is not possible to recreate the synchronization pattern again and thus to “recall the memory”. The above view of neuron synchronization patterns in the brain drives the need to explore the diversity of synchronization patterns produced by different connectivity schemes in neuron networks.

The coexistence of coherent with incoherent domains found in chimera states may offer an explanation of neurological states such as the unihemispheric sleep of animals [19, 20]. In maze-learning experiments it has been reported that rats show increased neural phase synchronization. Their decisions depend on previous knowledge of the environment which might have been retrieved from memory stores [21]. Phase synchronisation often coexists with chimera states, especially in complex neuron connectivity patterns.

After many decades of studying locally connected neuron oscillators, with and without time delays, recently nonlocal connectivity patterns have caught considerable attention. This was driven by the numerous applications of biological or technological interest which involve systems (networks) of many interacting components. It was made possible due to the fast development of computer resources which allows to tackle reliably networks consisting of a large number of units. In the classical nonlocal connectivity schemes each oscillator is linked to a number of elements $R_L \geq 1$ on the left and $R_R \geq 1$ on the right [1, 2, 7]. Mostly, the symmetric case $R_L = R_R$ was studied but asymmetric coupling ($R_L \neq R_R$) has recently been used to control the undesired erratic lateral motion of chimera states [22]. The case $R_L = R_R = 1$ corresponds to the local, nearest neighbor connectivity. The extension of connectivity to regions $R_L, R_R > 1$ led to the interesting phenomenon of chimera and in 2013 to multichimera states [9]. The interplay of nonlocal connectivity with the nonlinearity of the dynamical scheme has led to multiple incoherent domains and chimera death states [23–27]. In the recent years connectivity was further complexified to take into account results of diffusion tensor MRI analysis indicating that the neuron axons

distribution in the human brain (and thus the neuron connectivity) has hierarchical (fractal) connectivity [28–30]. These studies have revealed the pattern of nested chimeras [10] which also appears in systems of hierarchically arranged reactive units [31] and coupled Van der Pol oscillators [32]. Other nonlocal schemes include 2D (square lattice) and 3D (cubic lattice) connectivity with corresponding chimera patterns and are recently reported in [33, 34].

In previous studies synchronization phenomena have been explored in LIF networks using negative (repulsive) diffusive coupling with and without refractory period [35, 36]. We showed that in classical nonlocal coupling multichimera states emerge whose multiplicity (number of coherent/incoherent domains) depends both on the coupling strength and on the refractory period. We also showed that hierarchical topology in the coupling induces nested chimera states and transitions between multichimera states with different multiplicities. These results revealed new complex patterns and dynamical transitions between different multichimera states resulting from the combined effects of nonlinear dynamics with the hierarchical coupling. In the current study we use a different coupling pattern, the reflecting connectivity, in which each neuron is connected with a number of other neurons across a standard mirror diagonal of the ring. This idea stems from studies in the brain where neurons located on the surface of one hemisphere are connected with neurons arranged on the opposite hemisphere [18]. We give numerical evidence that such arrangements lead to multileveled incoherent states which coexist with near-threshold elements. Multileveled incoherent states are characterized by groups of elements having different mean phase velocities. These are novel interesting patterns and occur in LIF neurons when connected via reflecting coupling.

This work is organized as follows: In section II we recapitulate the main properties of the LIF model, and we study synchronization phenomena in coupled LIF elements with diffusive coupling when a finite refractory period is introduced. In section III we scan the parameter space and study the formation of domains with near-threshold elements and clustering phenomena. In section IV we investigate the effects of introducing reflecting connectivity matrices and study the resulting oscillation patterns and configuration transition phenomena. We give evidence of transitions between synchronous oscillations and chimera states with multileveled mean phase velocities, using as control parameters the coupling strength and the refractory period. In the concluding section we discuss possible applications of this study, we summarize our main results and discuss open problems.

II. LEAKY INTEGRATE-AND-FIRE MODEL WITH DIFFUSIVE COUPLING AND FINITE REFRACTORY PERIOD

The single neuron LIF model is common for excitatory and inhibitory dynamics and consists of a single linear differential equation describing the integration of the neuron potential $u(t)$, followed by a highly nonlinear, abrupt resetting of the potential to its ground value $u(t) = u_0$ [35]. Namely,

$$\frac{du(t)}{dt} = \mu - u(t) \quad (1a)$$

$$\lim_{\epsilon \rightarrow 0} u(t + \epsilon) \rightarrow u_0, \quad \text{when } u(t) \geq u_{\text{th}}. \quad (1b)$$

Equation (1a) represents the integration of the potential $u(t)$, which develops accumulating contributions with rate μ [37–40]. The term $-u(t)$ on the right hand side of this equation represents the “leaky term” which prohibits the neuron potential from increasing to arbitrarily large values, but forces it to converge to the value μ , for $t \rightarrow \infty$. An integral constituent of the single LIF model is Eq. (1b), which restores the potential $u(t)$ to its ground value u_0 every time the potential exceeds its upper threshold termed as “ u_{th} ”. This way a closed potential loop is created with extreme values $u_0 \leq u(t) \leq u_{\text{th}}$. Due to the structure of Eq. (1a), $u(t)$ can reach the value u_{th} and thus drop to the ground state u_0 only if $u_{\text{th}} < \mu$.

Equation (1a) is linear and can be solved analytically as long as the potential $u(t) \leq u_{\text{th}}$. The solution is:

$$u(t) = \mu - (\mu - u_0) \exp(-t), \quad \text{for } u(t) \leq u_{\text{th}}, \quad (2)$$

where, without loss of generality, we have assumed that at $t = 0$ the potential is at the ground state u_0 . The period T_s of the single neuron potential loop takes the following form, provided that the resetting to the ground potential is abrupt (has zero duration):

$$T_s = \ln \frac{\mu - u_0}{\mu - u_{\text{th}}}. \quad (3)$$

This period accounts exactly for the duration for the potential of a single (uncoupled) neuron to reach the threshold value u_{th} starting from the ground state u_0 . Because $u_0 < u_{\text{th}} < \mu$, the period T_s is always positive. Taking the constraints into account the general solution of the single LIF neuron can be written as:

$$\begin{aligned} u(t) &= [\mu - (\mu - u_0) \exp(-t_{T_s})] [1 - \delta(t - nT_s)], \\ t_{T_s} &= t \bmod T_s \\ n &= \frac{t - t_{T_s}}{T_s}. \end{aligned} \quad (4)$$

Biological neurons spend a resting period after firing each spike, which is called “refractory period”, p_r . This

is an essential feature of spiking neurons and we account for this by adding to the model Eq. (1) the following condition [35]:

$$u(t) \equiv u_0, \quad \forall t : [l(T_s + p_r) + T_s] \leq t \leq [(l + 1)(T_s + p_r)], \\ \text{where } l = 0, 1, 2, \dots \quad (5)$$

I.e. after each firing at times lT_s the neuron retains its potential to the resting state u_0 for an additional time interval p_r . With this additional condition, the total period T of the single neuron and corresponding frequency ω , including refractory time, are:

$$T = T_s + p_r = \ln \frac{\mu - u_0}{\mu - u_{\text{th}}} + p_r, \quad (6a)$$

$$\omega = \frac{2\pi}{T} = \frac{2\pi}{\ln \frac{\mu - u_0}{\mu - u_{\text{th}}} + p_r}. \quad (6b)$$

Having defined the single neuron dynamics we proceed by placing single neurons in a ring network and coupling them via two different schemes. The coupling topology as well as the coupling form are very important in neuron networks. Hereafter, we will use diffusive coupling, which is the simplest linear coupling and takes the form $[u_j(t) - u_i(t)]$ between neurons j and i . The coupling topology of the brain is very complex, as was discussed in the Introduction, hence in this study we will use two types of representative coupling: a) nonlocal coupling in section III and b) reflecting coupling in section IV. The topology is defined by the adjacency or connectivity matrix $\sigma(i, j)$ which is different in cases a) and b) as will be discussed in the corresponding sections. For a number of N LIF elements, each of them having potential $u_i(t)$, $i = 1, \dots, N$ and connected in a ring topology the network dynamics is described by the following scheme:

$$\frac{du_i(t)}{dt} = \mu - u_i(t) + \frac{1}{N_i} \sum_{j=1}^{N_i} \sigma(i, j) [u_j(t) - u_i(t)] \quad (7a)$$

$$\lim_{\epsilon \rightarrow 0} u_i(t + \epsilon) \rightarrow u_0, \quad \text{when } u_i(t) \geq u_{\text{th}} \quad (7b)$$

where N_i is the total number of elements that are linked to element i . In general, the number of elements N_i to which element i is linked may be different. In Eq. (7) we assume that all elements have as common parameters (properties) the refractory period p_r , the threshold potential u_{th} , the accumulating rate μ , while they start from different (usually random) initial states. Also in the current work we assume that the number of linking sites $N_i = N_c$ is kept constant for all elements. In later studies, these conditions need to be relaxed since in realistic biological neurons each neuron has different characteristics corresponding to its role in the brain functions [10, 26]. The +sign in front of the coupling term in

Eq. (7a) defines the attracting coupling dynamics. When u_i takes high values (higher than u_j) the coupling term becomes negative. This contribution tends to decrease the value of u_i (towards u_j) inhibiting its further growth. In the opposite case, when u_i takes lower values than u_j the coupling term $u_j(t) - u_i(t)$ becomes positive and this contribution tends to increase the value of u_i , towards u_j . Because the coupling term tends to bridge the differences between the interacting units we regard this coupling as “attracting”.

Synchronisation properties are quantitatively described by the mean phase velocity ω_i of element i . If the system is integrated for time ΔT , we compute the number of full cycles c_i which element i has completed during ΔT . The mean phase velocity of element i is then estimated as [9]:

$$\omega_i = \frac{2\pi c_i}{\Delta T} \quad (8)$$

Visually, synchronization patterns and chimera states are represented by the space-time plots. Space-time plots are colour coded plots that show the evolution of the potential of the oscillators in time and in space. These are particularly useful in the cases of transitions between different synchronization patterns, when the mean phase velocities do not give meaningful results.

Specifically for the LIF model it is necessary to introduce an additional quantitative index A which represents the ratio of elements below-threshold. This will become clearer in section III and Figs. 1, 3 and 5 where static and oscillatory elements coexist in the system. These partially static profiles indicate that many elements are confined near-threshold, while a few escape toward the resting potential $u_0 = 0$, see for example Fig. 1 (left panels). However, spacetime plots indicate that these “active” elements are not localized but the activity propagates from one element to the next around the ring. Thus the mean-phase velocity is not an appropriate measure of coherence, because each element spends some intervals of time near-threshold and other intervals in the “active” state (excursions below-threshold). Because in these cases the average number of below-threshold elements is statistically constant in time the representative quantitative index A of elements below-threshold is defined as:

$$A = \frac{1}{N\Delta T} \sum_{t=1}^{\Delta T} \sum_{i=1}^N q_i(t) \quad (9)$$

where

$$q_i(t) = \begin{cases} 1 & \text{when } u_i(t) < u_{\text{th}} \\ 0 & \text{otherwise.} \end{cases} \quad (10)$$

The index A counts the average number of elements that stay below-threshold and is calculated after the system has reached the steady state. Because it counts the number of active elements it is also referred to as “activity

factor”. Synchronisation properties in LIF coupled elements were studied in 2010 by Lucioli et al. [41] and Olmi et al. [42]. These studies have demonstrated the presence of chimera states in non-locally coupled LIF elements with time delays. In our work we further introduce a finite refractory period which is a well established characteristic of the biological neuron, and we also complexify the connectivity, which introduces the novel effect of the multileveled incoherent domains, as we will see in the section IV.

Without loss of generality, throughout this work the working parameters are kept to values $\mu = 1.0$, $u_{\text{th}} = 0.98$, $u_0 = u_{\text{rest}} = 0$. The system size is kept to $N = 1000$ elements.

III. EFFECTS OF NONLOCAL DIFFUSIVE COUPLING

In the case of nonlocal connectivity of the LIF elements arranged in a ring geometry, the matrix $\sigma(i, j)$ takes the form:

$$\sigma(i, j) = \begin{cases} \sigma & \text{for } i - R < j < i + R \\ 0 & \text{otherwise} \end{cases} \quad (11)$$

where σ is positive and all indices are understood mod (N). In this case the element i is linked with R other elements to its left and R elements to its right. The number of connections $N_i = N_c = 2R$, is equal for all elements. The dimensionless coupling range is defined as $r = R/N$ and represents the fraction of the system’s constituents contributing to the dynamics of each element. In the next subsection we present the synchronization phenomena observed as we vary the system parameters, the coupling range r , the coupling strength σ and the refractory period, p_r .

A. Variation of the coupling range

Using the nonlocal connectivity rules of Eqs. (7) we simulate a LIF ring network of $N = 1000$ oscillators and record the evolution of profiles and spacetime plots.

Figure 1 presents typical snapshots and spacetime plots of the system for different values of the coupling radius R and keeping the other parameters constant. All realizations shown in Fig. 1 start from the same initial conditions, $u_i(t = 0)$, $i = 1, \dots, N$, randomly chosen between 0 and u_{th} . The snapshots and spacetime plots show that the oscillators organize into spatial clusters where all elements remain close to the threshold while these regions are interrupted by oscillating regions in which the elements make excursions away from the threshold. In most cases examined the oscillating regions travel through the system with constant velocity. As the moving fronts on the right panels indicate, the velocity of the oscillating regions around the ring changes inversely with the parameter r .

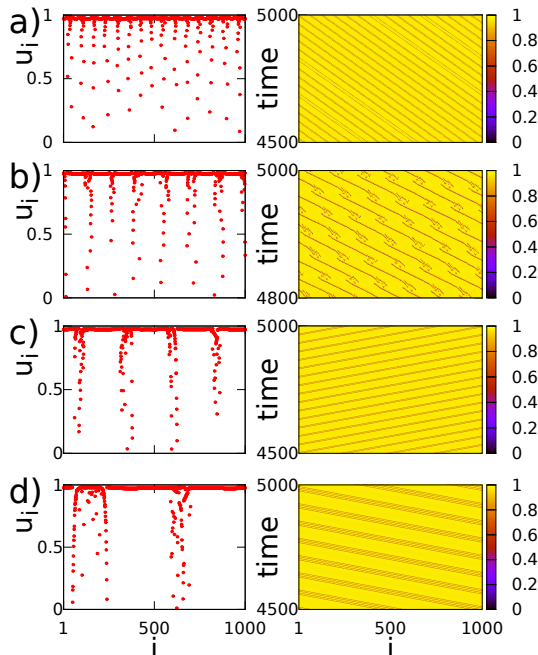


FIG. 1: (Color online) LIF system with nonlocal connectivity: Typical snapshots (left column) and spacetime plots (right column). a) $R = 50$, b) $R = 100$, c) $R = 200$, d) $R = 350$. Other parameters are $p_r = 0$, $\sigma = 0.7$, $N = 1000$, $\mu = 1$, and $u_{th} = 0.98$. All realizations start from the same initial conditions, randomly chosen between 0 and u_{th} .

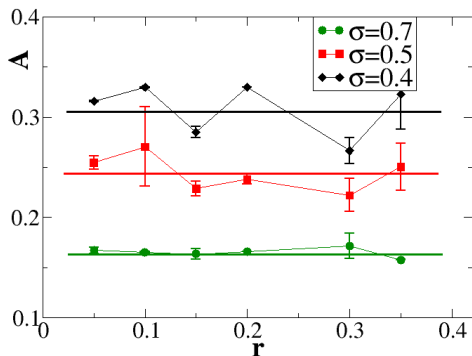


FIG. 2: (Color online) The activity factor A in the LIF system with diffusive nonlocal coupling as function of the coupling range $r = R/N$ and for $\sigma = 0.4$ (black line) $\sigma = 0.5$ (red line) and $\sigma = 0.7$ (green line). Averages are taken over 10 initial conditions. The straight lines are guides to the eye. Other parameters as in Fig. 1.

Figure 1a shows the formation of active domains alternating with domains where the elements stay near-threshold. The active (and near-threshold) domains move around the ring with constant velocity, as is indicated by the constant slopes in the corresponding

(right) spacetime plot. As the coupling range r increases, Fig. 1b,c, nearby oscillating domains merge into larger active clusters which are interrupted by threshold elements staying near potential u_{th} . This merging reduces the number of active N_a and near-threshold N_{th} domains, without violating (statistical) continuity around the ring. If we denote by $\langle N_a \rangle$ the average number of active domains and $\langle s_a \rangle$ the average size of each active domain, and similarly for the domains containing threshold elements, then the continuity condition around the ring is expressed by the conditions:

$$\begin{aligned} N_{th} &= N_a \\ \langle N_{th} \rangle \langle s_{th} \rangle + \langle N_a \rangle \langle s_a \rangle &= N \end{aligned} \quad (12)$$

where s_{th} and s_a are the sizes of the near-threshold and active domains, respectively. The size of the active clusters as well as the size of the near-threshold regions stay (statistically) constant in time. The oscillatory motion observed in Figs. 1a,c,d, i.e. a number of waves travelling at constant velocity in a sea (1D ring) of almost immobile elements, is reminiscent of soliton propagation in a medium, although the condition for solitons are not exactly met in this system. The difference with soliton phenomena is apparent in Fig. 1b, where the moving wave disappears while a new one is created in a nearby node. These patterns correspond to intermediate states which appear when the number of active (and near-threshold) domains changes and will be discussed further in section IIIB.

A counter-intuitive observation is that the number of active (below threshold) elements does not significantly depend on r . This can be seen in Fig. 2 where the fraction of below-threshold elements is calculated as a function of r . As a result, (see Fig. 1b,c,d) as r increases the elements are redistributed into equidistant clusters, while the distance (in threshold elements) between active clusters increases. More specifically, in Fig. 2 we present the fraction A of elements which are below the threshold as a function of r , for three different values of the coupling constant σ . The value A is calculated as the average (over time) fraction of elements which have potential $u_i \leq 0.97$. Average values (and error bars) are taken over 10 different initial conditions. In cases where the error bars are not visible, their size is smaller than the representing symbol. We observe that A stays constant, up to statistics. This means that the magnitude of activity in the system mostly depends on the strength of the coupling constant. While the coupling strength σ is related to the magnitude of the activity, the coupling range r is related to the organization of the activity in isolated regions and this might have important implications in the exchange of electrical signals between neurons.

B. Variation of the coupling strength

Modifications to the general activity of the system is also achieved with variations in the coupling constant

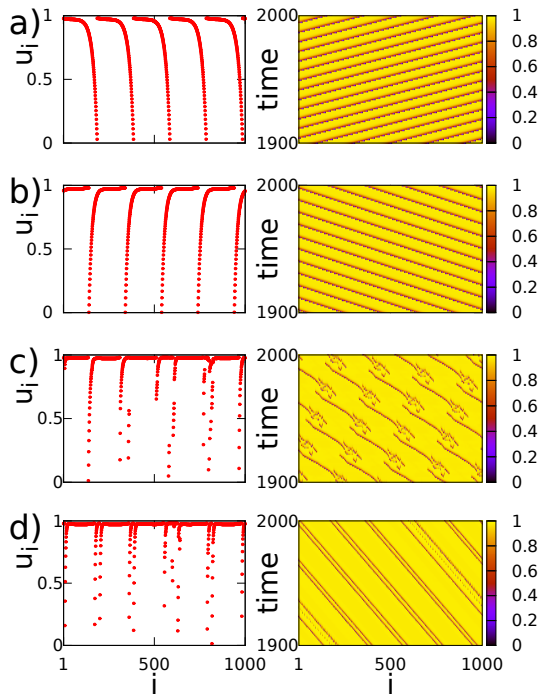


FIG. 3: (Color online) LIF system with nonlocal connectivity: Typical snapshots (left column) and spacetime plots (right column). a) $\sigma = 0.2$, b) $\sigma = 0.3$, c) $\sigma = 0.6$ and d) $\sigma = 0.7$. Other parameters are $p_r = 0$, $R = 150$, $N = 1000$, $\mu = 1.0$ and $u_{th} = 0.98$

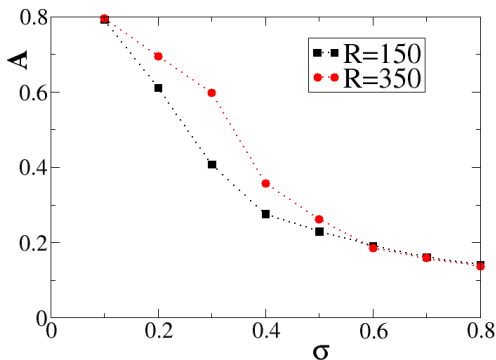


FIG. 4: (Color online) The activity factor A in the LIF system with diffusive nonlocal coupling as function of the coupling constant σ , for two different values of the coupling radius $R = 150$ (black squares) and $R = 350$ (red circles). Other parameters as in Fig. 1.

σ . In Fig. 3a, for small values of σ we observe synchronized waves propagating through the system. As the coupling strength increases the oscillators organize into near-threshold clusters. These clusters are interrupted by elements making abrupt excursions towards the resting potential $u_0 = 0$ (Fig. 3b). While for small values of σ the oscillators follow one-another keeping a constant

phase difference (Fig. 3 a,b), for large values of the coupling constant clusters are formed which travel around the ring with a constant velocity (Fig. 3d). The transition from the synchronized waves to the clusters occurs for intermediate parameter values, around $\sigma \sim 0.6$ for this working parameter set, as depicted in Fig. 3c. Here a wave disappears, but before disappearing it coexists with another one which has spontaneously been created at a nearby location. These hybrid states mediate (are at the turning point) between the simple moving waves and the clustered ones. As the parameter σ increases above 0.6 the regions of coexistence increase, forming gradually the clusters. These travelling clusters are separated again by near-threshold domains. The same effect was previously seen in Fig. 1b, between the simple active clusters (Fig. 1a) and the composite (grouped) ones (Fig. 1c and d). For the working parameters used in Fig. 1 the transition was recorded around $R = 100$, $\sigma = 0.7$, $p_r = 0$.

The activity factor A as a function of σ is shown in Fig. 4. We note a decrease in the number of elements making excursions below the threshold as the coupling strength grows. This can be intuitively understood as follows: The tendency of the oscillators to stay near the threshold is attributed to the exponential nature of the dynamics which tends asymptotically to μ as $t \rightarrow \infty$. As σ increases the system has the tendency to synchronize and thus more and more elements are attracted to stay near the threshold, and thus A decreases accordingly. As seen from Fig. 4 confirming Fig. 2, the value of the coupling range $r = R/N$ does not play a significant difference in the scaling of A . We note here that the splitting of the system in near-threshold and active domains is only observed in the case of attracting coupling where the elements are held to stay together near the threshold. This phenomenon is not observed in repulsive coupling, where more classic chimeras are supported [35, 36].

C. Variation of the refractory period

Similarly to Figs. 1 and Fig. 3, Fig. 5 displays variations in the snapshots and spacetime plots for different values of the refractory period, keeping all other parameters fixed. For these plots a constant $R = 150$ value was used.

The opposite effect is seen as the refractory period increases away from 0. For small values of p_r and for constant values of sigma $\sigma = 0.7$, Fig. 5a shows clustering of active oscillators. As also discussed in previous sections, IIIA and B, the clusters travel around the ring with a constant velocity as is clearly indicated by the corresponding spacetime plot. At the same time, all other elements take near-threshold values. As p_r increases the ratio of below-threshold elements A decreases, while the position of the clusters gets pinned in space, see Fig. 5b,c. The activity is anchored around specific points of the ring, fluctuating locally around them. As p_r increases the fluctuations decrease and as can be seen in Fig. 5d, only specific el-

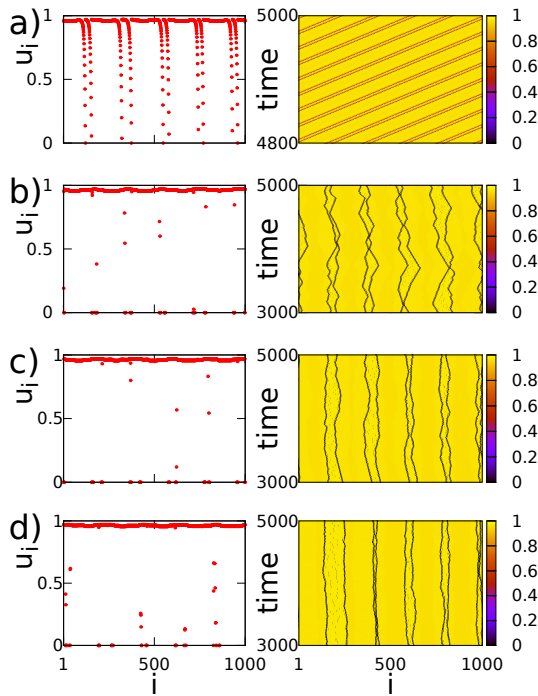


FIG. 5: (Color online) LIF system with nonlocal connectivity: Typical snapshots (left column) and spacetime plots (right column). a) $p_r = 0.01s$, b) $p_r = 0.3T_s$, c) $p_r = 0.5T_s$ and d) $p_r = 0.8T_s$. Other parameters are $R = 150$, $\sigma = 0.7$, $N = 1000$, $\mu = 1.0$ and $u_{th} = 0.98$.

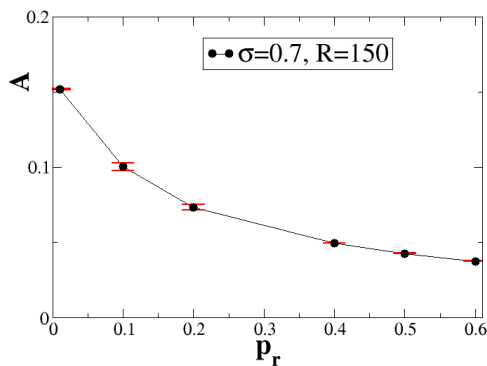


FIG. 6: (Color online) The activity factor A in the LIF system with diffusive nonlocal coupling as function of the refractory period p_r , for coupling radius $R = 150$. Averages are taken over 10 initial conditions. Other parameters as in Fig. 5.

elements make excursions away from the threshold. The decrease in the system activity is shown in Fig. 6, which displays the change of A as a function of p_r . Averages are taken over 10 different initial conditions. The refractory period induces a gradual, small decrease in the activity of the system, while pinning the position of the active elements. This effect has been verified for other values of

r and σ (not shown).

IV. EFFECTS OF REFLECTING COUPLING

In previous studies the influence of the complexity of the connectivity matrix on the steady state was investigated. In refs.[10, 31, 32, 35, 43] hierarchical connectivity was investigated giving rise to complex phenomena, such as hierarchical and traveling multichimeras and transitions between chimera states with different multiplicity. In this study we introduce a new type of connectivity, the mirror connectivity, or reflecting connectivity which is also inspired by the division of the brain in two symmetric hemispheres. Mirror connectivity means that neurons belonging to one hemisphere can connect with neurons in the other hemisphere and vice-versa. In this simplistic model where the LIF neurons are set in a ring architecture we assume that each neuron connects to its mirror image across a diagonal axis of the ring and to all the neurons belonging to a region of size R on the left and right of the mirror neuron, see Fig. 7. Without loss of generality and because of the cyclic symmetry of our ring, we assume that the diagonal axis for the mirror images is the one that passes from positions $k = N$ (top) and $k = N/2$ (bottom), as marked in Fig. 7. The reflecting connectivity matrix $\sigma(i, j)$ linking node j to i takes the form:

$$\sigma(i, j) = \begin{cases} 1 & \text{for } (N - i - R) < j < (N - i + R) \\ 0 & \text{otherwise} \end{cases} \quad (13)$$

Here also all indices are understood $\text{mod}(N)$. The above rules allow each LIF element to interact with the same, constant number of $2R$ elements with directed mirror links on the ring.

To investigate the effects of this connectivity scheme we fix the number of oscillators to $N = 1000$ and the number of links to $2R = 200$ ($R = 100$) and the refractory period to $p_r = 0$. The results are plotted in Fig. 8. Reflecting connectivity induces an unexpected phenomenon in the dynamics. From Fig. 8 we see that for small values of the coupling constant $\sigma < 0.3$ the system is synchronized and the potential variables u_i of all oscillators cover the entire range $0 \leq u_i < u_{th}$, which is allowed from the system constraints, Eq. (1). As σ increases, we observe a transition around the value 0.3, where the elements on the one half-ring remain close to the threshold while the ones in the other half-ring oscillate with variable mean phase velocities. We can say that this is a spatial coexistence of a coherent steady state domain with incoherent oscillations, because on the one side the elements do not oscillate and on the other side they oscillate but their mean phase velocities present modulations much like the ones observed in chimera states. In fact, the ω variations are more complex than in classical chimeras; as σ increases away from the transition the oscillators in the middle of the active semi-ring develop gradually a convex shape with a minimum in the middle

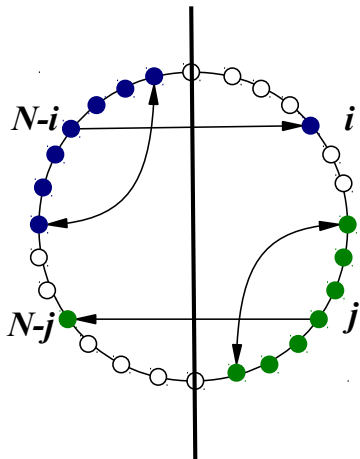


FIG. 7: (Color online) Schematic representation of the mirror connectivity around the diagonal passing from neurons set at positions N (top node) and $N/2$ (bottom node). For simplicity only the connectivity of element at position i on the top-right (blue elements) and of element $N-j$ on the bottom-left (green) are depicted. The connectivity of all other elements (including the white ones) is not shown.

of the active semi-ring, Fig. 8c and d. The maximum value of the mean phase velocity remains constant, the depth of the convex shape increases with σ as can be seen in Fig. 8e, where the ω_{max} and ω_{min} values are depicted. As we increase further the coupling strength a secondary ω peak develops in the middle of the active region (Fig. 8d), where the oscillators speedup with respect to their neighbors. For this value of coupling radius $R = 100$ the size of the active region seems to remain almost constant as a function of σ . This is not always the case, as we show evidence in the sequel. Incoherent states with complex modulation in their mean phase velocities were previously observed in the FitzHugh-Nagumo model, when the single chimeras are transformed into multichimeras as the coupling range r increases [9]. The difference with the current study is that here the multichimera states coexist with a number of near-threshold oscillators and this is due to the combined effect of reflecting connectivity and positive (attracting) coupling dynamics. Another difference to Ref. [9] is that the modulations here take place when the coupling constant σ changes, while in Ref. [9] multiplicity of the chimera increases as r increases.

To explore further the influence of this connectivity in the system synchronization, we choose to examine the same features for a large value of coupling radius, $R = 300$. Figure 9 shows that for small values of σ we have the synchronized regime, around $\sigma = 0.2$ a first destabilization takes place where the system splits into two pairs of mutually synchronous regions, around $\sigma = 0.3$ only one of the semi-rings stays active, while in the other one the oscillators stay near the threshold

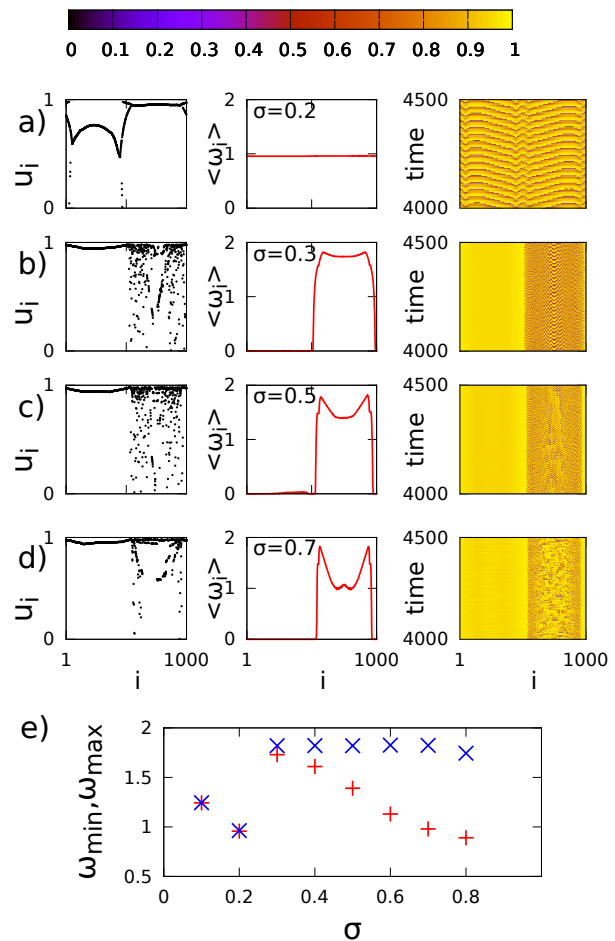


FIG. 8: (Color online) LIF system with reflecting connectivity and varying coupling constant σ . Typical snapshots are depicted in the left column, mean phase velocities in the middle and spacetime plots in the right column. a) $\sigma = 0.2$, b) $\sigma = 0.3$, c) $\sigma = 0.5$, d) $\sigma = 0.7$, e) ω_{min} and ω_{max} as a function of σ . Other parameters are $N = 1000$, $R = 100$, $\mu = 1$ and $u_{th} = 0.98$ and $p_r = 0$. All realizations start from the same, randomly selected initial conditions between 0 and u_{th} .

and do not venture away from it. As before, near the threshold the mean phase velocity profile on the semi-ring achieves an arc-like shape, while as σ increases a plateau starts developing. For even larger values of σ the convex shape is formed in the middle of the active region (not shown). Comparison between panels 9c and 9d indicates that the active region, where excursions away from the threshold take place, shrinks with σ . Figure 9e depicts the size of the active region A as a function of σ . For small σ all $N = 1000$ elements are active. Around $\sigma = 0.3$ a transition takes place and the active region is confined in one of the two semi-rings. The active region shrinks further as σ increases.

To prompt further into the properties of this system we study the dependence on the coupling radius R , keeping the coupling strength constant, $\sigma = 0.4$, and other

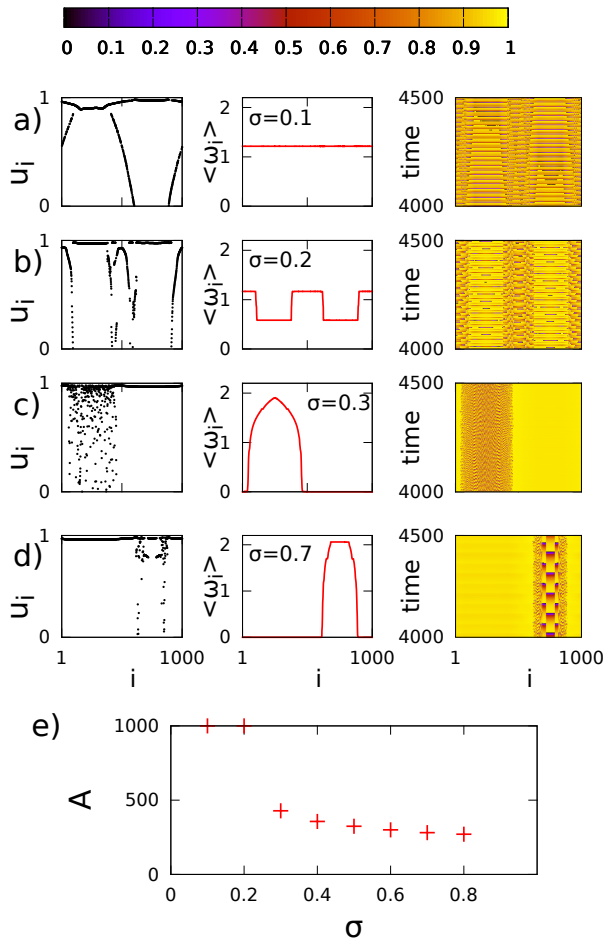


FIG. 9: (Color online) LIF system with reflecting connectivity similar to Fig. 8 and $R = 300$. a) $\sigma = 0.2$, b) $\sigma = 0.3$, c) $\sigma = 0.5$, d) $\sigma = 0.7$, e) Size of the active region A as a function of σ . All other parameters as in Fig. 8.

parameter values as in the previous figures. In Fig. 10 we can see that even for small R -values, as small as 10, the activity is isolated into one of the two semi-rings, with abrupt change of behaviour at the interfaces. Counter-intuitively, as the coupling radius increases the width of the active stripe decreases up to a limit value of R , which for these parameter values is in the range $300 \leq R_{\text{lim}} \leq 350$, Fig. 10c. Note that for this limiting value the ω -shape in the active semi-ring takes the arc form. For large values of $R > R_{\text{lim}}$ the spreading of the coupling in larger regions causes oscillations in both parts of the system, Fig. 10. The symmetry in the reflecting connectivity can be seen in the mean phase velocity plots: the oscillations in both semi-rings are images of one another. Coherent oscillations are developed in the middle of each semi-ring while the elements which border the semi-ring connections are out-of-order (incoherent). As we increase further the coupling radius the incoherent regions shrink, while the system synchronizes completely. In this respect, increasing the coupling radius or the

coupling constant causes different effects in the system: when the coupling radius R increases the system passes from (active-passive) semi-rings to (active-active) semi-rings; when the coupling constant σ increases the system passes from the (active-active) phase to the (active-passive) one with simultaneous shrinking of the active phase.

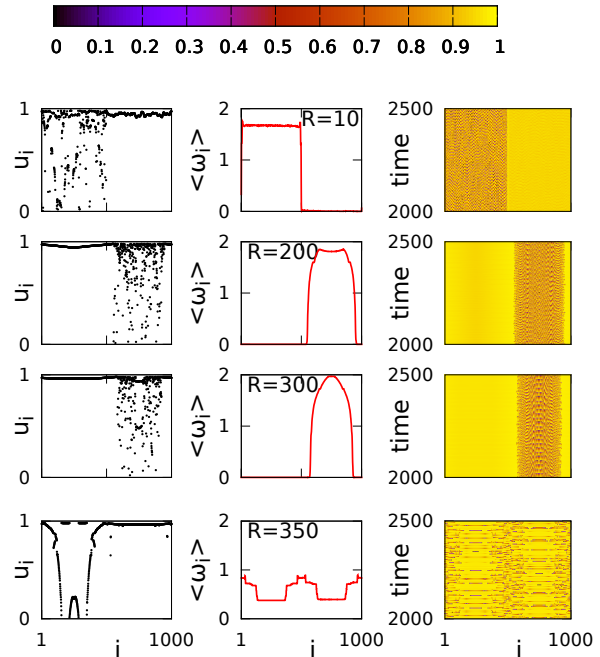


FIG. 10: (Color online) LIF system with reflecting connectivity with varying coupling radius R . Typical snapshots are depicted in the left column, mean phase velocities in the middle and spacetime plots in the right column. a) $R = 10$, b) $R = 200$, c) $R = 300$, d) $R = 350$ and e) $R = 400$. $\sigma = 0.4$ $p_r = 0$ and other parameters as in Fig. 8.

We next consider variations in the refractory period p_r in Fig. 11 keeping other parameters fixed to $R = 100$ and $\sigma = 0.4$. For $p_r = 0$ the system keeps the usual convex semi-ring arrangement as was also observed previously for the variations with R , see Fig. 10. As p_r increases the convex arrangement deepens, while around $p_r \sim 0.4T_s$ the mean phase velocity develops 2 minima of similar structure. This behaviour persists for larger values of p_r , until around $p_r \sim 0.7T_s$ where a second transition takes place and the active domain splits into three smaller active ones which now reside in both semi-rings. The introduction of the refractory period thus induces multiple coherent and incoherent regions, separated by the near-threshold elements. These three regions persist for even larger values of p_r . Transient states (not shown) with two active stripes were observed but they were short-living turning into either the single stripe or to the structure with three stripes.

Finally, we take a closer look at the near-threshold elements. These elements are not entirely fixed but fluctuate near the threshold potential. Fig. 12 shows the

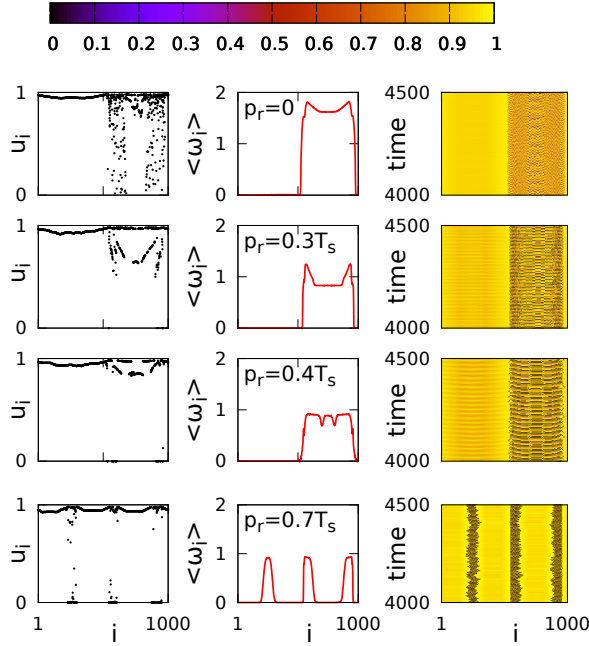


FIG. 11: (Color online) LIF system with reflecting connectivity with varying refractory period p_r . Typical snapshots are depicted in the left column, mean phase velocities in the middle and spacetime plots in the right column. a) $p_r = 0$, b) $p_r = 0.3T_s$, c) $p_r = 0.4T_s$, and d) $p_r = 0.7T_s$. $R = 100$, $\sigma = 0.4$ and other parameters as in Fig. 8.

temporal behaviour of the element $i = 35$ in the cases of $p_r = 0, 0.1T_s, 0.3T_s$ and $0.4T_s$, with all other parameters as in Fig. 11. This figure provides evidence that the threshold elements fluctuate with higher amplitude as the refractory period increases.

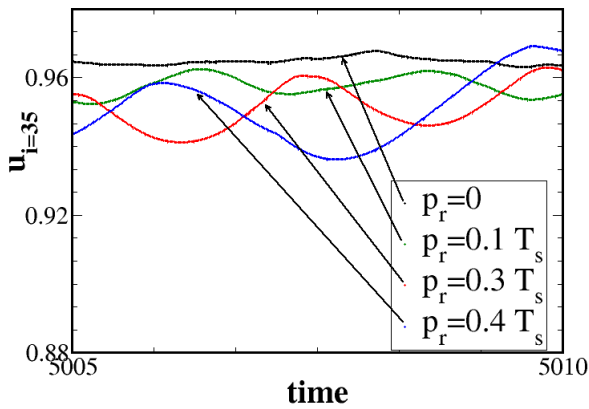


FIG. 12: (Color online) Temporal evolution of the potential u of threshold LIF elements. Lines depict the fluctuations of element $i = 35$, for $p_r = 0$ (black line), $p_r = 0.1T_s$ (green line) $p_r = 0.3T_s$ (red line) and $p_r = 0.4T_s$ (blue line). $R = 100$, $\sigma = 0.4$ and other parameters as in Fig. 11.

Overall, the introduction of a reflecting connectivity architecture induces restriction of the oscillations on a single domain which resides in one half of the ring, while in the other half the elements remain close to the threshold potential u_{th} . Within the active domains the oscillators organize in domains with different phase velocities and transition regions. The introduction of a common refractory period to all LIF elements induces splitting of the single active domain into smaller ones; these smaller active stripes reside in both ring semi-circles.

V. CONCLUSIONS

Synchronisation phenomena in diffusively coupled Leaky Integrate-and-Fire elements are examined in the case of nonlocal coupling and reflecting connectivity. In the case of the classical nonlocal diffusive coupling traveling waves of synchronous elements with constant phase difference are observed, while chimera states are difficult to identify. Due to the travelling of the waves all elements spent some part of the time in the coherent and part in the incoherent regions and thus the difference in the mean phase velocity, which is the signature of the chimera states, smears out. The number of oscillators which are below the threshold is statistically constant in time and only depends on the parameter values σ and p_r . In the case of reflecting connectivity evidence is produced for novel incoherent domains coexisting with near threshold elements. This phenomenon is observed in the coupled model when each element is connected with elements in its mirror across a diagonal axis. For this connectivity, the oscillations are restricted in one half of the ring, while the elements of the other half stay near the threshold. For small values of the coupling constant σ the oscillatory activity covers the entire ring. As σ increases the activity is restricted in one of the semi-rings while the size of the active region decreases inversely with σ . If a refractory period is added to the system the single activity regions split, the active regions are spread in both semi-rings and they are separated by near-threshold elements

In the current study we assume that all elements are identical, i.e., they have common parameters: the coupling constant σ , the refractory period p_r , the threshold potential u_{th} and the accumulating rate μ . In further studies these assumption can be relaxed and different parameters can be assigned to the elements/neurons, depending on their physiology and functioning. Furthermore, one can add inhomogeneity in the form of a small dispersion around a mean value, to any of these parameters and study the implications of this statistical variation in the form and properties of the chimera states.

Topology-connectivity is also relevant in neurological disorders (schizophrenia, Alzheimer, Parkinson etc). In some of them the damage may be hereditary, in others it may develop with age. In all these cases it is important to understand how connectivity changes with previous expe-

rience, disorder and age and how this influences/modifies the network synchronization patterns. The outcome of research in this direction will be twofold: on the one hand the relation between neuronal network architecture and brain functionality (perception and memory) can be established and on the other hand the association of connectivity with brain disorders will be elucidated. MRI and resting vs. task oriented fMRI experiments are expected to shed light in these important issues.

VI. ACKNOWLEDGMENTS

This work was supported by the German Academic Exchange Service (DAAD) and the Greek State Scholarship

Foundation IKY within the PPP-IKYDA framework. Funding was also provided by NINDS R01-40596. The research work was partially supported by the European Union's Seventh Framework Program (FP7-REGPOT-2012-2013-1) under grant agreement n316165. PH and ES acknowledge support by DFG in the framework of the Collaborative Research Center 910. JH acknowledge support in the framework of the SIEMENS program "Establishing a Multidisciplinary and Effective Innovation and Entrepreneurship Hub". This work was supported by computational time granted from the Greek Research & Technology Network (GRNET) in the National HPC facility - ARIS - under project ID PA002002.

-
- [1] Y. Kuramoto and D. Battogtokh, Coexistence of coherence and incoherence in nonlocally coupled phase oscillators, *Nonlinear Phenomena in Complex Systems* **5**, 380 (2002).
- [2] D. M. Abrams and S. H. Strogatz, Chimera states for coupled oscillators, *Phys. Rev. Lett.* **93**, 174102 (2004).
- [3] M. J. Panaggio and D. Abrams, Chimera states: coexistence of coherence and incoherence in networks of coupled oscillators, *Nonlinearity* **28**, R67 (2015).
- [4] E. Schöll, Synchronization patterns and chimera states in complex networks: interplay of topology and dynamics, *Eur. Phys. J. Spec. Top.* **225**, 891 (2016).
- [5] C. R. Laing and C. C. Chow, Stationary bumps in networks of spiking neurons, *Neural Computation* **13**, 1473 (2001).
- [6] H. Sakaguchi, Instability of synchronized motion in nonlocally coupled neural oscillators, *Phys. Rev. E* **73**, 031907 (2006).
- [7] I. Omelchenko, Y. Maistrenko, P. Hövel and E. Schöll, Loss of coherence in dynamical networks: Spatial chaos and chimera states, *Phys. Rev. Lett.*, **106**, 234102 (2011).
- [8] J. Hizanidis, V. Kanas, A. Bezerianos and T. Bountis, Chimera states in networks of nonlocally coupled Hindmarsh-Rose neuron models, *Int. J. Bifurcation Chaos* **24**, 1450030 (2014).
- [9] I. Omelchenko, O. E. Omel'chenko, P. Hövel and E. Schöll, When nonlocal coupling between oscillators becomes stronger: patched synchrony or multichimera states, *Phys. Rev. Lett.* **110**, 224101 (2013).
- [10] I. Omelchenko, A. Provata, J. Hizanidis, E. Schöll and P. Hövel, Robustness of chimera states for coupled FitzHugh-Nagumo oscillators, *Phys. Rev. E* **91**, 022917 (2015).
- [11] J. Hizanidis, N. E. Kouvaris, G. Zamora-López, A. Díaz-Guilera and C. G. Antonopoulos, Chimera-like states in modular neural networks, *Sci. Rep.* **6**, 19845 (2016).
- [12] R. G. Andrzejak, C. Rummel, F. Mormann and K. Schindler, All together now: Analogies between chimera state collapses and epileptic seizures, *Scientific Reports* **6**, 23000 (2016).
- [13] N. Brunel and M. C. W. Van Rossum, Lapicques 1907 paper: from frogs to integrate-and-fire, *Biol. Cybern.* **97**, 337-339 (2008).
- [14] R. A. Poldrack and M. J. Farah, Progress and challenges in probing the human brain, *Nature* **526**, 371-379 (2015).
- [15] N. K. Logothetis, What we can do and what we cannot do with fMRI (Review), *Nature* **453**, 869-878 (2008).
- [16] S. Ruiz, N. Birbaumer and R. Sitaram, Abnormal neural connectivity in schizophrenia and fMRI-brain-computer interface as a potential therapeutic approach, *Front. Psychiatry* **4**, 17 (2013).
- [17] E. Hannon et al., Methylation QTLs in the developing brain and their enrichment in schizophrenia risk loci, *Nature Neuroscience* **19**, 48-54 (2016).
- [18] E. S. Finn et al. Functional connectome fingerprinting: identifying individuals using patterns of brain connectivity, *Nature Neuroscience* **18**, 1664-1671 (2016).
- [19] N. C. Rattenborg, C. J. Amlaner, and S. L. Lima, Behavioral, neurophysiological and evolutionary perspectives on unihemispheric sleep, *Neurosci. Biobehav. Rev.* **24**, 817 (2000).
- [20] N. C. Rattenborg, B. Voirin, S. M. Cruz, R. Tisdale, G. DellOmo, H.-P. Lipp, M. Wikelski and A. L. Vyssotski, Evidence that birds sleep in mid-flight, *Nature Communications* **7**, 12468 (2016).
- [21] J. Fell, N. Axmacher, The role of phase synchronization in memory processes, *Nature Reviews Neuroscience* **12**, 105-118 (2011).
- [22] I. Omelchenko, O. Omel'chenko, A. Zakharova, M. Wolfrum and E. Schöll, Tweezers of chimeras in small networks, *Physical Review Letters* **116**, 114101 (2016).
- [23] A. Zakharova, M. Kapeller and E. Schöll, Chimera Death: Symmetry Breaking in Dynamical Networks, *Phys. Rev. Lett.* **112**, 154101 (2014).
- [24] I. Schneider, M. Kapeller, S. Loos, A. Zakharova, B. Fiedler and E. Schöll, Stable and transient multi-cluster oscillation death in nonlocally coupled networks, *Phys. Rev. E* **92**, 052915 (2015).
- [25] T. Banerjee, Mean-field-diffusion-induced chimera death state, *Europhysics Letters* **110**, 60003 (2015).
- [26] S. A. M. Loos, J. C. Claussen, E. Schöll and A. Zakharova, Chimera patterns under the impact of noise, *Phys. Rev. E* **93**, 012209 (2016).
- [27] T. Banerjee, P. Sharathi Dutta, A. Zakharova and E. Schöll, Chimera patterns induced by distance-dependent power-law coupling in ecological networks,

- Phys. Rev. E **94**, 032206 (2016).
- [28] P. Katsaloulis, D. A. Verganelakis and A. Provata, Fractal dimension and lacunarity of tractography images of the human brain, *Fractals* **17**, 181-189 (2009).
- [29] P. Expert, R. Lambiotte, D. Chialvo, K. Christensen, H. J. Jensen, D. J. Sharp and F. Turkheimer, Self-similar correlation function in brain resting-state functional magnetic resonance imaging, *Journal of the Royal Society Interface* **8**, 472-479 (2011).
- [30] P. Katsaloulis, A. Ghosh, A. C. Philippe, A. Provata and R. Deriche, Fractality in the neuron axonal topography of the human brain based on 3-D diffusion MRI, *European Physical Journal B* **85**, 150 (2012).
- [31] J. Hizanidis, E. Panagakou, I. Omelchenko, E. Schöll, P. Hövel and A. Provata, Chimera states in population dynamics: Networks with fragmented and hierarchical connectivities, *Phys. Rev. E* **92**, 012915 (2015).
- [32] S. Ulonska, I. Omelchenko, A. Zakharova and E. Schöll, Chimera states in hierarchical networks of Van der Pol oscillators, *Chaos* **26**, 094825 (2016).
- [33] Y. Maistrenko, O. Sudakov, O. Osiv and V. Maistrenko, Chimera states in three dimensions, *New J. Phys.* **17**, 073037 (2015).
- [34] O. Omel'chenko, M. Wolfrum, S. Yanchuk, Yu. Maistrenko, O. Sudakov, Stationary patterns of coherence and incoherence in two-dimensional arrays of non-locally coupled phase oscillators, *Phys. Rev. E* **85**, 036210 (2012).
- [35] N. D. Tsigkri-DeSmedt, J. Hizanidis, P. Hövel and A. Provata, Multi-chimera states in the Leaky Integrate-and-Fire model, *Procedia Computer Science* **66**, 13 (2015).
- [36] N. D. Tsigkri-DeSmedt, J. Hizanidis, P. Hövel and A. Provata, Multi-chimera states and transitions in the Leaky Integrate-and-Fire model with nonlocal coupling and hierarchical connectivity, *European Physical Journal, Special Topics* **225**, 1149 (2016).
- [37] B. Ermentrout, Neural networks as spatio-temporal pattern-forming systems, *Rep. Prog. Phys.* **61**, 353-430 (1998).
- [38] R. D. Vilela and B. Lindner, Comparative study of different integrate-and-fire neurons: Spontaneous activity, dynamical response, and stimulus-induced correlation, *Phys. Rev. E* **80**, 031909 (2009).
- [39] B. B. Lindner, L. Schimansky-Geier and A. Longtin, Maximizing spike train coherence or incoherence in the leaky integrate-and-fire-model, *Phys. Rev. E* **66**, 031916 (2002).
- [40] N. Kouvaris, F. Müller and L. Schimansky-Geier, Ensembles of excitable two state units with delayed feedback, *Phys. Rev. E* **82**, 061124 (2010).
- [41] S. Luccioli and A. Politi, Irregular collective behavior of heterogeneous neural networks, *Physical Review Letters* **105**, 158104 (2010).
- [42] S. Olmi, A. Politi and A. Torcini, Collective chaos in pulse-coupled neural networks, *Europhys. Lett.* **92**, 60007 (2010).
- [43] T. Isele, J. Hizanidis, A. Provata and P. Hövel, Controlling chimera states: The influence of excitable units, *Phys. Rev. E* **93**, 022217 (2016).